ELSEVIER

Polymer 42 (2001) 8787–8798

polymer

www.elsevier.com/locate/polymer

Self-nucleation and enhanced nucleation of polyvinylidene fluoride (α-phase)

S. Schneider[a], X. Drujon[b], B. Lotz[a], J.C. Wittmann[a,*]

[a]*Institut Charles Sadron, CNRS-ULP, 6 rue Boussingault, 67083 Strasbourg, France*
[b]*ELF-Atochem, Groupement de Recherche de Lacq, Route 177, B.P. 34, 64170 Lacq, France*

Received 12 December 2000; received in revised form 9 May 2001; accepted 11 May 2001

Abstract

The nucleation phenomena of poly(vinylidene fluoride) in its α-phase (α-PVDF) are investigated. Self-seeding first investigated helps establish a so-called 'efficiency scale', which in turn helps rate the nucleation induced by crystalline additives, and notably PTFE. The thermal and nucleation behavior of α-PVDF is significantly dependent on its microstructure. Samples with higher head-to-head inversions display a significant 'memory effect': their initial spherulitic morphology is maintained in successive recrystallizations. The nucleation density can be increased by addition of nucleating agents: PTFE or flavanthrone. The nuclei densities reached are, however, nearly two orders of magnitude lower than for isotactic polypropylene. These results serve as a basis for a companion investigation of the nucleation of blends of PVDF and polyacrylic polymers, the structural characteristics and properties of which can be significantly modified by enhancing nucleation.

Keywords: Poly(vinylidene fluoride); Crystallization; Nucleating agents

1. Introduction

Control of the spherulite size by addition of nucleating agents is an easy means to modify and adapt the physical properties of bulk crystalline polymers to specific end uses. For example, addition of derivatives of sorbitol to isotactic polypropylene imparts transparency, as a result of significant reduction of spherulite size [1]. Friedrich [2] has also shown that as a result of mechanical impact, crazes develop first in large spherulites, and only later in smaller ones.

Reduction of spherulite size is also a major concern for materials such as poly(vinylidene fluoride) (PVDF) [3], which are used as protective layers and coatings, i.e. must sustain long term use, often under severe physical conditions and chemical environments, and/or hard-to-reach locations (underwater cables, etc.).

The present paper and its companion [4] investigate the self-nucleation and enhanced nucleation of PVDF and blends of PVDF and poly(methylmethacrylate) (PMMA). The self-nucleation is analyzed following a methodology already used for isotactic polypropylene (iPP) [5–7]. It rests on the analysis of the impact of partial melting of the samples on subsequent recrystallization as investigated in a DSC apparatus, and helps establish a so-called 'efficiency scale' for nucleation additives of PVDF. An unexpected outcome of this investigation is the observation of specific morphological effects (i.e. a 'memory effect') [6] linked most probably with variations of the chemical architecture of the samples.

Enhanced heterogeneous nucleation of PVDF is achieved by use of its two known nucleating agents: flavanthrone [8] and poly(tetrafluoroethylene) (PTFE) [9]. The physical interactions between polymer and nucleating agent are investigated, and the overall efficiencies of the latter are determined with the help of the efficiency scale.

In the companion paper [4], the procedures and concepts are applied to blends of PVDF with compatible amorphous polymers, which are used as components of paints and for which aspect properties (e.g. gloss), also highly dependent on spherulite size, are essential. It will be shown that the impact of nucleating agents is more dramatic for these industrially relevant systems than for the homopolymer PVDF.

2. Materials and experimental techniques

2.1. Materials

Three different grades of commercial latexes of PVDF produced by ELF-Atochem are used: Kynar® 500, 740

* Corresponding author. Tel.: +33-3-8841-4021; fax: +33-3-8841-4020.
E-mail address: wittmann@ics.u-strasbg.fr (J.C. Wittmann).

0032-3861/01/$ - see front matter
PII: S0032-3861(01)00361-5

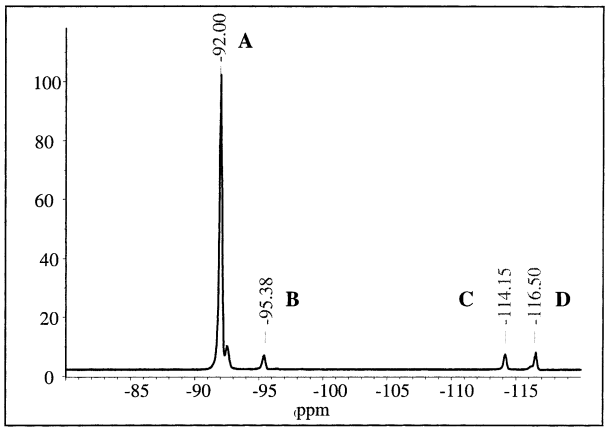

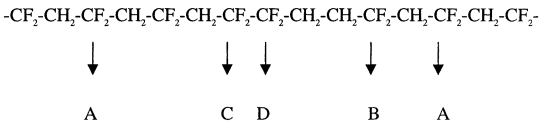

Fig. 1. ^{19}F NMR spectra at 200 Hz of Kynar 740 sample: 4% (w/w) solution in a 50/50 (v/v) mixture of DMAc and acetone-d_6 and assignment of the peaks according to Ref. [11].

and 1000. Kynar 740 and 1000 are polymerized at relatively low temperature in order to limit head to head defects, i.e. increase the regioregularity. The molecular weights (M_w) are controlled by a chain transfer agent added during polymerization and are nearly similar (≈175,000 g/mol) (as determined by GPC at the King of Prussia facility of ELF Atochem North America). Kynar 500, being polymerized at higher temperature and without chain transfer agent, is more regiodefective and its molecular weight is (presumably) higher. Its exact M_w cannot, however, be determined by GPC since the polymer is only partly soluble.

The regioregularity of the samples is characterized by ^{19}F nuclear magnetic resonance (NMR) spectroscopy using a Bruker 200 MHz instrument. 4% (w/w) PVDF solutions in mixtures of DMAc and acetone-d_6 (50/50) are used. The determination follows the analyses of Lutringer et al. [10] who showed that the reversal rate can be determined from ^{19}F NMR spectra, with first order Markov statistics. As an illustration, the ^{19}F NMR spectrum of Kynar 740 shown in Fig. 1 displays four well-resolved peaks for which the assignment of the pentads is unambiguous [11]. Only the first peak corresponds to perfect regioregular sequence: $-CF_2-CH_2-CF_2-CH_2-CF_2-$, whereas the three other peaks correspond to different regioregularity defects. The molecular characteristics of the three samples are summarized in Table 1.

Powders of commercial PVDF from Solvay, Solef 1001 and extruded sheets of Kureha PVDF were also used to build up a meaningful diagram relating reversal rate and melting temperatures for the various Kynar grades.

A latex of PTFE, and flavanthrone (ICI) of commercial origin are used as nucleating additives.

Table 1
Head to head defect concentration and corresponding melting temperatures for the different PVDF samples

Sample	Head–Head (%)	T_m (°C)
Kynar 500	5.5	162.0
Kynar 1000	4.8	168.9
Kynar 740	4.7	169.0
Solef	4.2	174.2
Kureha	3.9	175.4

2.2. Sample preparation

The samples, initially in a latex form, are first coagulated by freezing. About 20 g of latex are slowly frozen at −5°C for 6 h, and then stored overnight at room temperature. The destabilized latexes are centrifuged at 20,000 rpm for 10 min and the precipitated polymer is redispersed and washed three times in distilled water (to eliminate the surfactants used in the polymerization), centrifuged, and dried during 24 h at 50°C under vacuum.

In one set of experiments designed to investigate the impact of the microstructure, the soluble and insoluble parts of Kynar 500 were separated. The procedure involves partial 'dissolution' of the polymer powder in dimethylacetamide (DMAc) (10%, w/w) at room temperature with agitation. After several hours, the solution is centrifuged at 20,000 rpm for 6 h, leaving a soluble fraction in the supernatent, and the insoluble fraction at the bottom of the tube in a 'gel' form. The two fractions are re-precipitated in an excess of distilled water, filtered, washed and dried following the protocol described above.

The nucleating additives are blended in different ways with PVDF. Flavanthrone is only available in powder form, and is blended with the PVDF latex. The procedure is even simpler for PTFE: since both PVDF and PTFE exist in the form of latexes, they are mixed prior to precipitation and drying.

2.3. Experimental techniques and procedures

DSC investigations are performed in a Perkin–Elmer DSC4 instrument fitted with a thermal analysis data station (TADS). About 10 mg of polymer powder are sealed in aluminum pans. Heating and cooling rates are usually set at 10 K/min, and the time spent at T_s (partial melting temperature) is 5 min. All melting or crystallization temperatures are taken at the extremum of the peaks.

Morphological observations are performed by optical microscopy and light scattering. Samples suitable for OM observations are produced by using the original microtomy technique developed by Fillon et al. [5]: after crystallization in the DSC, the samples extracted from their aluminum pans are microtomed in sections ≈ 5 μm thick. This technique allows correlation between the morphology and the DSC investigations. Optical microscopy (OM) is performed in

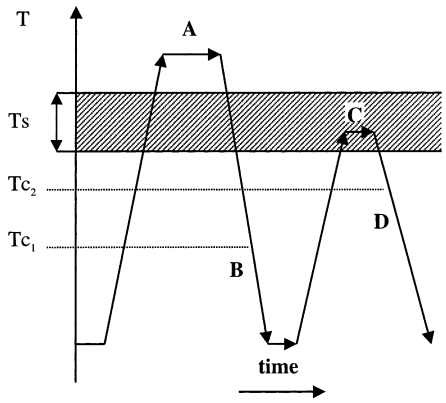

Fig. 2. Self-nucleation procedure as applied in the DSC apparatus. PVDF self-nucleating domain (shaded) is explored for heating and cooling rates of 10 K/min, steps A and C last 10 and 5 min, respectively. The positions of the crystallization peaks depend mainly for T_{c1} on sample characteristics, and for T_{c2} on these characteristics plus the partial melting conditions at T_s (step C). For step C, temperature domains above, in and below the shaded area correspond to complete melting, self-seeding, and annealing (domains I, II and III in Fig. 3), respectively.

polarized light using a Zeiss Photomicroscope II. Small angle light scattering (SALS) is specifically performed to analyze the memory effect and determine the spherulite size, but cannot be performed on the same DSC samples, since it requires much larger samples than sections of the material contained in the DSC pan. Solutions of PVDF in dimethylacetamide (DMAc) (20%, w/w) are therefore cast as thin films with a doctor blade apparatus at 65°C. They are crystallized in a heating stage (Mettler FP82 equipped with a temperature programmer) and examined by SALS in a home-made apparatus. They yield the familiar cloverleaf patterns (but also on occasions highly unconventional ones), which help determine the spherulite diameter from the position of the intensity maximum. As different preparation procedures and thermal inertia of equipment, sample geometry, etc. are involved, DSC and optical microscopy on one hand, and SALS on the other often yield slightly different spherulite sizes. However, comparison of morphology or size for different PVDF remains meaningful for any given set of crystallization conditions and observation.

Interactions between the nucleating species and PVDF are investigated by electron microscopy and electron diffraction. Flavanthrone crystals, even when crystallized under mild conditions, are ill defined and too small to perform any meaningful electron diffraction work. Bilayers of PTFE and PVDF are produced as follows: thin films of PTFE are produced by the by now familiar friction-transfer process [12,13]. A rod of PTFE is pressed against a glass slide heated at 350°C with a pressure of 1.5×10^6 Pa and moved at 0.25 mm/min. The PTFE film is ≈20–25 nm thick, and the chains are aligned parallel to the deposition axis. A PVDF film is prepared by evaporation from a solution in DMAc on a glass slide, floated off on water, and transferred onto the oriented glass supported PTFE layer. The composite film is heated for a few minutes at 200°C, i.e. above the melting temperature of PVDF but below that of PTFE, and quenched to room temperature. The samples are gold-decorated to enhance the defect lines and lamellar structure of PVDF, coated with carbon, and stripped off the glass substrate with the help of a polyacrylic acid backing. The samples are examined in a Philips CM12 microscope operated at 120 kV.

3. Results

3.1. Background: self-nucleation in the DSC and efficiency scale

Self-nucleation involves the partial melting of a 'standard' state of the polymer, followed by recrystallization using as nuclei the unmelted crystal fragments produced in the partial melting [13–15]. Four steps are necessary and are summarized in Fig. 2 [5–7].

- The prior thermal history is erased (A) by heating at a temperature $T > T_m$ (typically 200°C for PVDF) for 10 min. This treatment leaves only heterogeneous (hereafter referred to as residual) nuclei of unknown nature in the sample.
- In the second step (B), a standard easily reproducible state is generated by cooling at a constant rate (−10 K/min). The position of the crystallization peak, located at T_{c1}, depends on structural characteristics of the polymer that affect the spherulite growth rate G (M_w distribution, tacticity) and on the residual germ concentrations. This temperature is therefore a sample characteristic.
- The third, essential step (C), is a partial melting. The sample is heated to a selected temperature T_s close to, but lower than the (full) melting temperature T_m. As already mentioned, in this work the heating rate is 10 K/min and the sample is maintained at T_s for 5 min. The actual value of T_s is very critical: the number of unmelted crystal fragments increases sharply with decreasing T_s.
- In the fourth step (D), the sample experiences a second and last crystallization while being cooled at 10 K/min. The crystallization peak is located at a temperature T_{c2} higher or at most equal to T_{c1}. The increase in T_c reflects the increase in nuclei concentration resulting from partial melting at T_s.
- Yet an additional, fifth step can be introduced: it is a final melting, which helps characterize the structures formed in the fourth step, and detect the possible presence of a sizeable portion of unmelted and annealed material left during the partial melting (step three). This final step is essential in our definition of the acceptable lower T_s temperature, which should not leave a crystalline fraction detectable as an additional melting peak at high temperature. Although somewhat arbitrary, this

criterion corresponds actually to nuclei concentrations in the samples beyond which the enhanced nucleation process 'saturates': the nuclei density becomes too high to induce any significant further increase of the crystallization temperature.

The procedure just described makes it possible to define, on a conventional DSC melting curve, three domains of T_s corresponding to three different behaviors of the recrystallized polymer.

1. T_{s1} corresponds to the lower limit of complete melting. For any melting above this temperature, the number of thermally stable 'residual' heterogeneous nuclei remains constant and minimal, and subsequent cooling simply reproduces the standard state with its crystallization peak at T_{c1}.
2. For the intermediate T_s range, i.e. $T_{s2} < T_s < T_{s1}$, the polymer is partially melted. In this range, a decrease in T_s results in an increase of T_c on subsequent cooling. The increase reflects the increased concentration of crystalline fragments that survived the partial melting and act as nuclei. This concentration increases up to T_{s2} and the corresponding crystallization temperature T_{c2} characterizes the crystallization of a polymer melt saturated with nuclei that have ideal interactions (physical and chemical) with the crystallizing polymer. T_{c2} corresponds therefore to the highest crystallization temperature that can be reached for the sample by monitoring the nuclei concentration, dispersion, structure and compatibility within the melt.
3. Heating at temperatures $T_s < T_{s2}$ results in incomplete melting. The unmelted, annealed fraction shows up on a subsequent second melting (step 5) as an additional high temperature melting peak.

The above experiments can also be used to design a very convenient efficiency scale for nucleating additives [6]. Indeed, heating at T_{s1} and T_{s2} generates two polymer melts, which are 'loaded' with either the minimum number of nuclei (the residual ones) or the maximum achievable number of nuclei, which furthermore are ideal in terms of interactions with the polymer melt (same nature), dispersion (fragments of lamellae) and interactions with the crystalline phase (same crystal lattice). They provide therefore the lower T_{c1} and upper T_{c2} limits of T_c, i.e. the domain of T_c, $\Delta T_{c\,max} = T_{c2} - T_{c1}$. A heterogeneously nucleated sample will crystallize, say at $T_{c\,nucl}$, which is located within this temperature range. It is higher than T_{c1} (the sample is nucleated) but lower than T_{c2}, since the heterogeneous nuclei are not expected to be as compatible and/or as dispersed and/or as good crystalline substrates for the polymer melt as self-nuclei. The increase in T_c induced by the nucleating additive, i.e. $\Delta T_c = T_{c\,nucl} - T_{c1}$ can be scaled relative to the maximum range of T_cs, $\Delta T_{c\,max} = T_{c2} - T_{c1}$ and leads to a 'percentage of efficiency', defined by:

$$\text{Efficiency}\ (\%) = 100(\Delta T_c/\Delta T_{c\,max})$$

$$= 100(T_{c\,nucl} - T_{c1})/(T_{c2} - T_{c1})$$

The self-seeding process and efficiency scales are determined in the investigation of the crystallization behavior of PVDF examined now. This investigation reveals marked differences in terms of melting and crystallization behavior depending on the microstructure of the samples, but also indicates more subtle variations evidenced by the morphological observations.

3.2. Melting temperature and self-nucleation ranges of PVDF

3.2.1. Melting temperature as a function of molecular architecture

As a first step in the analysis of the crystallization behavior of PVDF, we examine first their melting behavior. Indeed, the crystallization and melting behaviors of PVDF are very sensitive to their microstructure, i.e. to the presence of head to head defects, which increases with the polymerization temperature [2]. As shown in Table 1, such variations are also observed with the Kynar samples, as well as for the Solef and Kureha samples with higher regioregularity (head to head contents of 4.2 and 3.9%, respectively). Although the absolute variations in defect concentrations appear small, they have a significant impact on the melting temperatures (taken here for the samples in their 'standard state', i.e. after melting beyond T_{s1} and crystallization at 10 K/min). Indeed, the melting temperatures range from 162 to 175.4°C. A plot of these melting temperatures versus the head to head defect concentrations determined by NMR (Table 1) indicates a linear relationship. This relationship can further be used to evaluate the regioregularity of samples, or even of fractions of samples that cannot be dissolved. The relationship applies for Kynar 740 and 1000, which have comparable defect concentrations (4.7 and 4.8%) and very similar melting temperatures. Throughout this investigation, however, we have observed consistent differences between Kynar 500 and the Kynar 740 and 1000 samples, as displayed also by their self-nucleation behavior (cf. later). As far as Kynar 500 is concerned, the plain polymer (not the fraction) with only slightly more defects (5.5%) has a significantly lower melting temperature. On this basis also, the melting temperature of the insoluble part of Kynar 500 suggests that this fraction has a 5.8% defect concentration.

3.2.2. Self-seeding domains as a function of molecular architecture

The above comparison of melting peak temperatures deals with only one aspect of the melting behavior of the polymers. Comparison of the self-seeding domains makes it possible to cover the broader spectrum of thermal stabilities

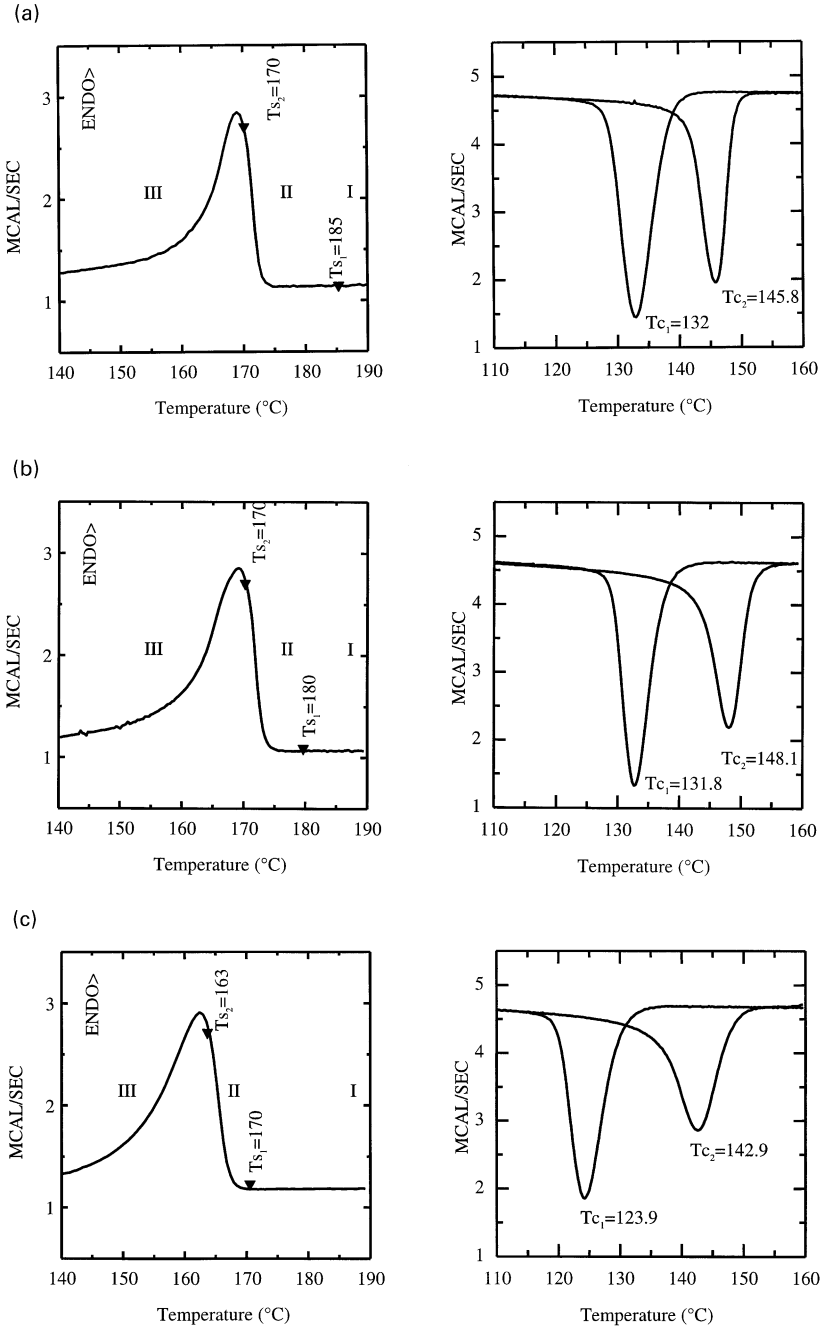

Fig. 3. Melting curves (with indication of the domains of melting (I), self-seeding (II), and annealing (III)) and crystallization curves for Kynar 740 (a), Kynar 1000 (b) and Kynar 500 (c), which helped build Fig. 2. Crystallization curves with peaks at T_{c1} and T_{c2} correspond to samples self-nucleated at the lower and higher limits of domain II on the melting curves, respectively (i.e. at T_{s1} and T_{s2}).

of crystals present in any given polymer sample. In particular, the self-seeding domains depend on the most stable fragments, which would be undetectable by global techniques (such as DSC), but are revealed by their role as nucleation sites on further cooling. Two criteria may be used to define this nucleation range: the magnitude of the range, i.e. $\Delta T_s = T_{s1} - T_{s2}$, and its position relative to the melting peak. It is worth recalling that (i) ΔT_s is rather narrow for isotactic polypropylene (4°C) [5–7] and even more so for polyethylene (1.5°C) [16], and (ii) the domain is usually located between the high temperature foot of the melting peak and its maximum.

The PVDF display a significantly different behavior. As shown in Fig. 3, the ΔT_s ranges are very large: 15°C for Kynar 740 (170–185°C), and 10°C for Kynar 1000. For these two samples, the curious feature is the respective positions of the self-nucleating and melting domains. The upper limits in particular (T_{s1}) are way outside the melting

curve (Fig. 3a and b), which suggests that the samples contain a very small fraction of very high molecular weight (and melting temperature), which is mainly involved in the self-nucleation.

Kynar 500 (Fig. 3c) is characterized by a narrower T_s range of only 7°C, and its position within, but on the higher side of the melting curve is better in line with previous observations on iPP and PE.

3.3. Crystallization behavior of PVDF: morphology, memory effect and correlation with the microstructure

3.3.1. Nuclei concentrations

In an earlier investigation of iPP self-nucleation, it was shown that the DSC crystallization curve can, to a good approximation, be treated as an isothermal crystallization at the peak temperature [6,7]. Given the cooling rate (10 K/min) and the breadth of the crystallization endotherm (about 10°C), the crystallization half time is 1/2 min. It is then possible to use the simplification of the Avrami equation applicable for the crystallization half-time, $t_{1/2}$ and deduce the rate constant K:

$$K_{t1/2} = (4\pi/3)NG^3$$

and ultimately, knowing the linear growth rate of spherulites G (measured by optical microscopy during isothermal crystallization experiments), determine the concentration of nuclei, N, per cm^3 of the polymer melt.

Note, however, that the proportionality of $K_{t1/2}$ and NG^3 assumes that the crystallization amounts to the development of hard spheres. The actual crystallization process may be geometrically more complex:

1. For high concentrations of nuclei, the growing entities may never reach the stage of three-dimensional spherulites, when they impinge with neighbors while they are still spherulite 'precursors'. These are elongated, fan-shaped objects, for which assuming three-dimensional growth geometry is inadequate. For the highest nuclei concentrations, the calculation therefore yields nuclei concentrations of a 'spherulitic-equivalent' of the actual crystalline morphology. Note also that the same restriction applies when the dispersion of nuclei in the melt is not random, as for e.g. nuclei organized in strings.
2. The spherulites grow as open textures, with much non-crystalline material remaining between the 'leading' lamellae (in Bassett's [19] terminology). This material crystallizes behind the growth front of spherulites. This 'retarded' crystallization within the spherulites appears, however, to have limited impact on the evaluation of nuclei. In the lower concentration range (corresponding to fully developed spherulites), the calculated nuclei concentration can indeed be assessed from the spherulite diameters. The method is, admittedly, rather blunt since the average spherulite diameter varies as $N^{1/3}$: a 10-fold increase in nuclei concentration is manifested by only a $10^{-3} = 2.15$ decrease in spherulite diameter. In any case, and keeping in mind that the nuclei concentrations cannot be determined with extreme accuracy, the agreement reached with experiment is satisfactory, which validates the procedure and the model on which it rests.

For the three samples of PVDF investigated, the ranges of crystallization temperatures $\Delta T_{c\,max} = T_{c2} - T_{c1}$ are relatively wide: 16.3, 13.8 and 19°C for Kynar 1000, 740 and 500, respectively. They are much wider than observed in PE (only 5°C) but inferior to those observed for iPP: 25°C. These ranges depend critically on the temperature variation of the growth rate (as also vividly illustrated in the companion paper). Indeed, since these experiments are performed at constant cooling rate and the shape of the crystallization endotherm is similar, the crystallization half-times $t_{1/2}$ remain constant (and equal to 30 s in our experiments): all the crystallization cycles are performed at constant 'rate constant' of the Avrami equation, or iso-K. In other words, the decrease of the growth rate G for higher crystallization temperatures is exactly compensated by the increase in the density of nucleation sites.

When applying this reasoning to the various PVDF samples investigated in this study, a rather constant behavior emerges. It can be summarized in a simple statement: the 'spontaneous' concentration of heterogeneous, permanent nuclei in the various PVDF is nearly the same, and is on the order of 10^7 germs/cm^3. Note that this figure is about one order of magnitude larger than for iPP, or, for that matter, for standard PEs. However, the nuclei concentration increases by only three to four orders of magnitude as a result of the self-nucleation procedure (up to about 10^{10}–10^{11} germs/cm^3). This increase is significantly less than for self-nucleated iPP or PEs: over six orders of magnitude (from 10^6 to 10^{12} for iPP) [6]. There is no good justification for this limitation, which suggests a possible clustering of the crystalline fragments in the self-seeded melt, or else indicates that our (somewhat arbitrary) definition of the lower limit of T_s, T_{s2}, should be revised. In the present case, for reasons which are not yet clear (especially in the light of the memory effect discussed next), the most efficient self-seeding procedure generates only one active nucleus per $\approx(4\ \mu m)^3$ (4 μm being the minimum size of the spherulites, formed after self-nucleation at T_{s2}).

3.3.2. Memory effects

3.3.2.1. Memory effect in Kynar 740 and 1000. Beyond the spherulite size of the various PVDF just examined, microscopic observations indicate a complicated pattern associated with the so-called memory effect, which takes usually place in the lower temperature range of the self-nucleation domain.

Let us recall this effect in its most standard manifestation, as illustrated for Kynar 740 in Fig. 4 (Kynar 1000 has a

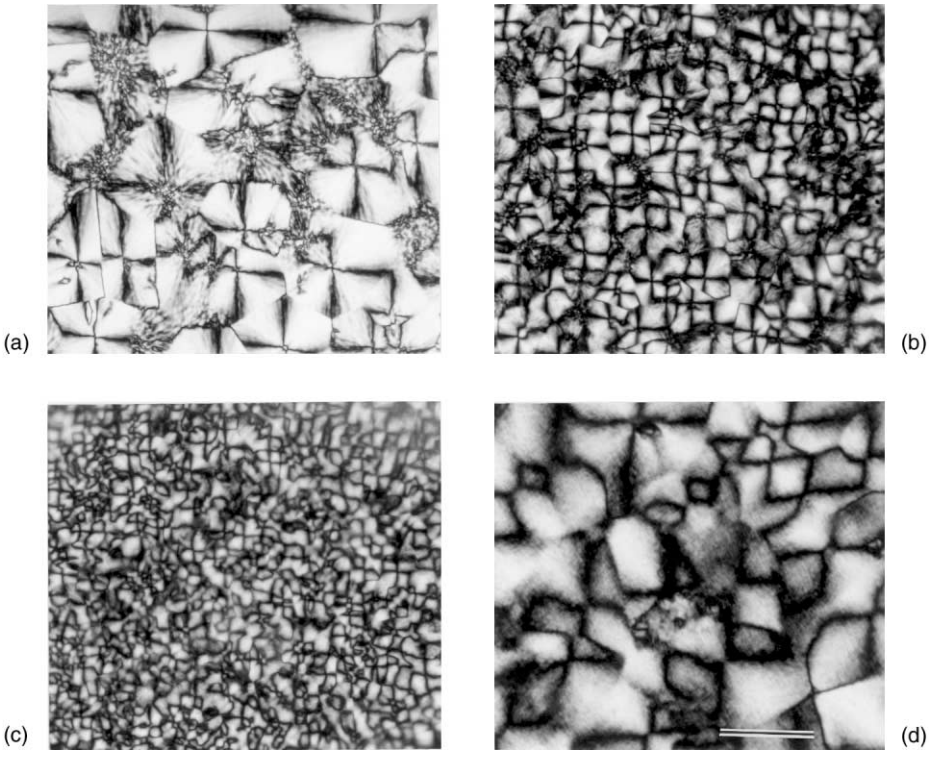

Fig. 4. Optical micrographs (crossed polars) of Kynar 740 crystallized after different T_s: (a) 200°C; (b) 176°C; (c) 172°C; (d) 170°C. Note the progressive reduction in spherulite size for decreasing T_s, and the apparent reversal of this trend for Fig. 4d. The latter figure corresponds to the onset of the memory effect (see text). Scale bar: 50 μm.

similar behavior, and will not be detailed; the unexpected behavior of Kynar 500 is considered next).

Fig. 4 illustrates the spherulitic morphologies after recrystallization of Kynar 740 submitted to decreasing T_s. The spherulite size initially decreases, as expected from the increase in the concentration of (self-) nuclei. At one point, however, in the lower part of the T_s range, the spherulites appear to be large again (Fig. 4d): they are actually similar to those of the standard sample (Fig. 4a). The self-nucleation treatment appears to have preserved the initial morphology. However, the crystallization temperature is much higher, and therefore the nuclei concentration is, by necessity, much larger than for the standard state. This behavior has been described as a memory effect [5–7]. It indicates that in this lower part of the T_s domain, the crystal fragments, which are left during the partial melting keep the memory of the orientation of the lamellae from which they originate. On subsequent cooling, initial lamellar growth on these fragments results in fan-shaped entities, which later evolve in small spherulites. Since the fan-shaped parts may represent a sizeable part of the recrystallized material and the orientation of their building lamellae is locally similar to that of the 'parent' spherulite, the contours of the parent spherulite are re-created — thus the term memory effect. The large recrystallized spherulites appear to 'remain' after the self-seeding treatment, since the initial spherulitic pattern is preserved. Their structure is, however significantly different, since they are by now 'fragmented' into a large number of smaller spherulites, even though the latter maintain (in combination) the overall pattern of the former.

While optical microscopy easily reveals the memory effect, it is of little use when it comes to determining the size of the smaller entities. Small angle light scattering (SALS) is of great help, and PVDF provides a particularly illustrative example of this contribution. Fig. 5a represents the classical cloverleaf-like H_v pattern for a sample self-nucleated at $T_s = 172$°C (corresponding optical micrograph: Fig. 4c). Fig. 5b represents the H_v pattern of Kynar 740 crystallized after self-nucleation at $T_s = 170$°C (corresponding optical micrograph: Fig. 4d). Whereas the optical micrograph shows only the larger sized spherulites, the SALS pattern (Fig. 5b) displays two superposed cloverleafs: a smaller one 'inserted' in a bigger one, which are due to the 'apparent' large spherulites and the 'true' smaller spherulites, respectively. It is the combination of optical microscopy and these SALS experiments, which makes it possible to determine the variation of spherulite size with T_s over the whole self-nucleation domain, as reported in Table 2.

Finally, it should be mentioned that the range of T_s ($\Delta T_{s\,ME}$) over which the memory effect (ME) takes place is quite narrow, in particular when compared with the very wide range over which the self-nucleation is active in PVDF. For Kynar 740 and 1000, the memory effect appears only in the lower 2°C of the self-nucleation domain, which is 15°C wide. As a comparison, for polyethylene the

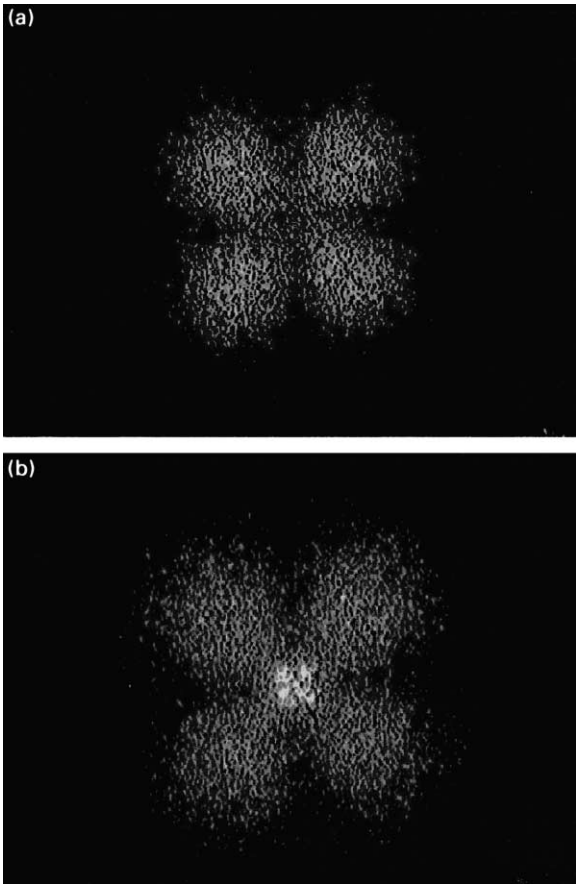

Fig. 5. Illustration of the memory effect by light scattering. H_v patterns for Kynar 740 crystallized after self-nucleation at $T_s = 172$°C (a) and $T_s = 170$°C (b). Note the extra, large angle clover-leaf indicating the existence of smaller crystalline entities produced by the self-seeding procedure (but not resolved by optical microscopy). As a result of the memory effect, the larger spherulites outlines remain visible in optical microscopy (Fig. 4d) and produce the smaller cloverleaf in light scattering.

memory effect appears in only the lower 0.5°C out of 3.5°C self-nucleation domain. For iPP (α-phase) corresponding figures are 2 and 4°C, respectively. Whereas Kynar 740 and 1000 are therefore quite standard, the behavior of Kynar 500 is definitely unusual since it displays a permanent memory effect, as examined now.

3.3.2.2. Permanent memory effect in Kynar 500 and gel fraction. When Kynar 500 is submitted to the self-nucleation procedure, a curious — and so far unique — behavior is brought to light (Fig. 6): there is no variation of the apparent spherulite size over the whole T_s range, in spite of the fact that, as judged by the increase in T_c, the nucleation process is effective: SALS data indicate indeed that the smaller spherulite diameters reached are as low as 4 μm. This unexpected result indicates that for Kynar 500,

Table 2
Spherulite size for the Kynar 740 sample submitted to different melting/self-nucleation experiments (T_s indicated). The nuclei concentration is deduced from the spherulite size. Note the two spherulite diameters for $T_s = 170$°C, corresponding to the memory effect (cf. also Figs. 4d and 5b)

T_s (°C)	200	176	172	170
T_c (°C)	132.0	137.5	141.2	145.8
Ø (μm)	50	25	16	38/4
N (germs/cm^3)	1.5×10^7	1.1×10^8	4.8×10^8	4.1×10^{10}

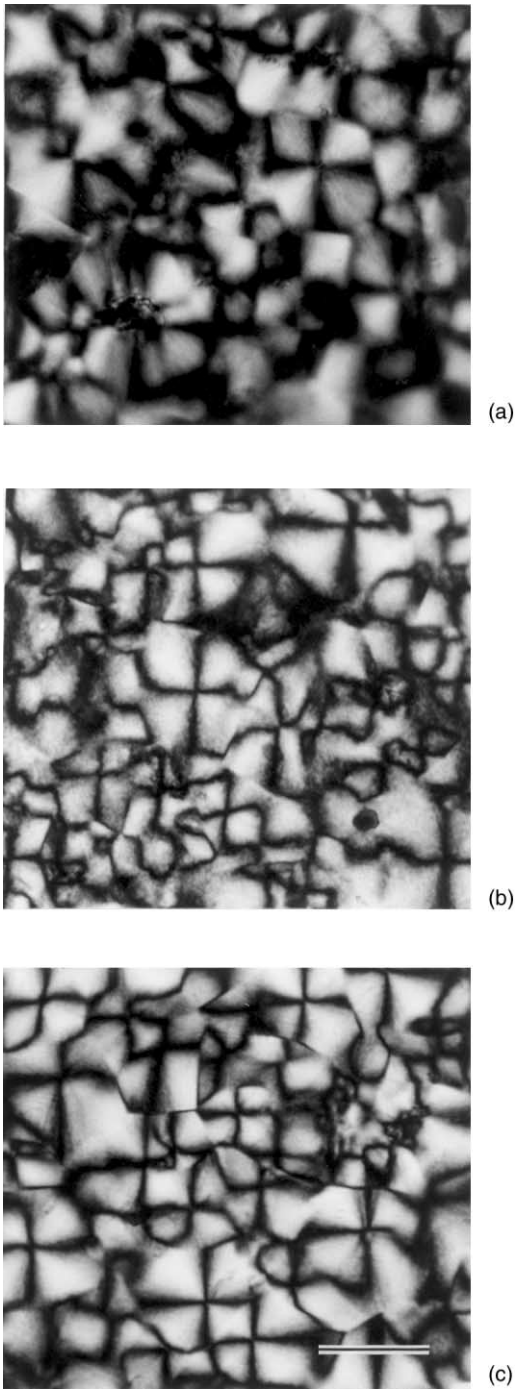

Fig. 6. Permanent memory effect of Kynar 500. Optical micrographs (crossed polars) of Kynar 500 crystallized after self-nucleation at 200°C (a), 168°C (b) and 163°C (c). Although the crystallization peak varies with T_s (cf. Fig. 3c), the spherulitic outline remains unaffected. Scale bar: 50 μm.

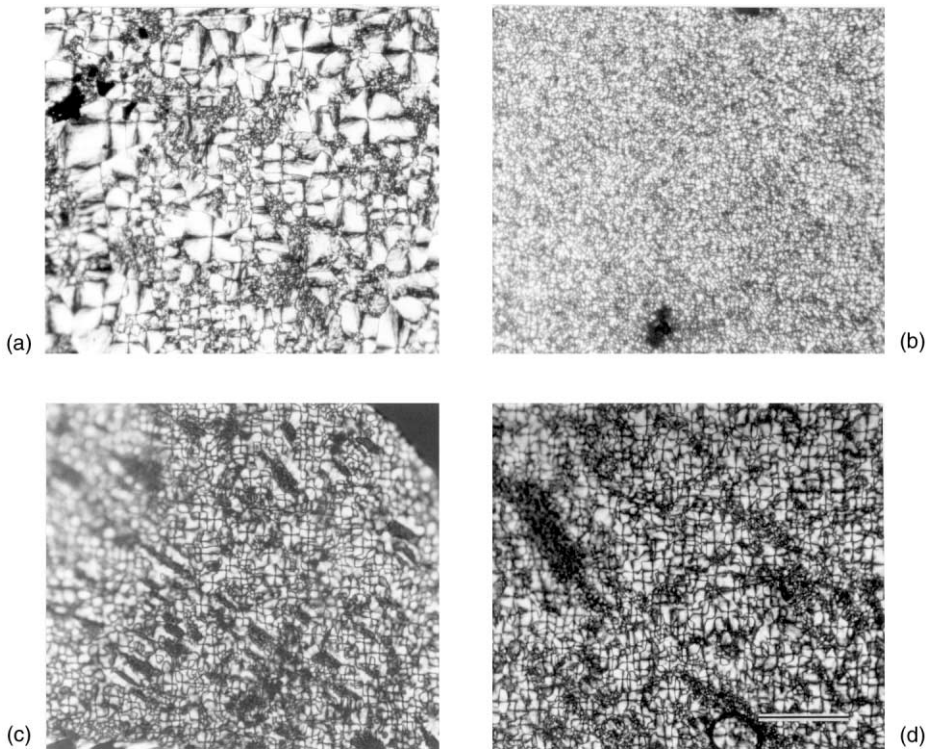

Fig. 7. Erasure and preservation of the permanent memory effect. Morphologies produced by self-nucleation of the soluble ((a) and (b)) and insoluble ((c) and (d)) fractions of Kynar 500 after melting (parts a and c) or self-nucleation at 164°C (b and d). In the soluble part the memory effect is lost: the spherulite diameter varies, whereas the memory effect remains for the insoluble part: the spherulite diameter remains constant. Scale bar: 50 μm.

the memory effect is permanent and extends over the whole self-nucleation range. Only melting at 200°C for 10 min restores a 'pristine' melt and generates a new spherulitic pattern.

The origin of the permanent memory effect is not fully understood at present. The molecular architecture of the polymer appears, however, to be a contributing, and perhaps an essential factor of this memory effect. From our earlier experience with PE [17], it appears that the presence of a small fraction of high M_w material is a trigger for the memory effect. In PEs, however, melting for prolonged times at the upper T_s annihilates the memory effect. This is not the case with the PVDF and in particular with the Kynar 500 sample, in which therefore yet a different origin, or at least a different contributing factor, must exist.

Our extensive investigations on the possible origin of this 'permanent memory effect' of Kynar 500 make it possible to establish a correlation with the microstructure of the sample. The observations and argument run as follows:

Kynar 500 is more regiodefective than the two other samples. Although the difference in absolute values is small, Kynar 500 cannot be completely dissolved and always leaves an insoluble gel fraction. Existence of this gel fraction can be unambiguously correlated with the memory effect through a simple test experiment, in which the soluble and insoluble parts are separated by centrifugation. The recrystallization behavior of the soluble part after annealing in its T_s range is standard, with the normal variation of spherulite size with T_s (Fig. 7a and b). To the contrary, the insoluble part always displays the permanent memory effect. Therefore, for Kynar 500 at least, the memory effect can be associated with the existence of a gel structure (Fig. 7c and d), which is maintained in the melt, and preserves the orientation of the crystalline fragments produced on self-nucleation.

Whether the gel itself is a nucleating species or not, or why this particular fraction does form a gel is not understood. However, Lutringer et al. [10] have established a clear relationship between microgel formation and microstructure of the PVDF fractions. They showed that the formation of a microgel in PVDF is associated with a higher fraction of reversed head to head addition and, furthermore, to a higher probability for not repairing a defect of reverse addition by an adjacent tail to tail addition. It was indeed confirmed by NMR that the insoluble fraction of Kynar 500 has more defects than either the soluble or the pure Kynar 500. This particular microstructure is locally an alternating ethylene–tetrafluoroethylene sequence, the copolymer of which melts indeed at very high temperature: 270°C. This microstructure could well act as a thermally stable net (if inactive) or as germs (if they are active nucleating species) due to a higher melting point of the microdomains. However, no good experimental tools are available to demonstrate this hypothesis, since the mass fraction of

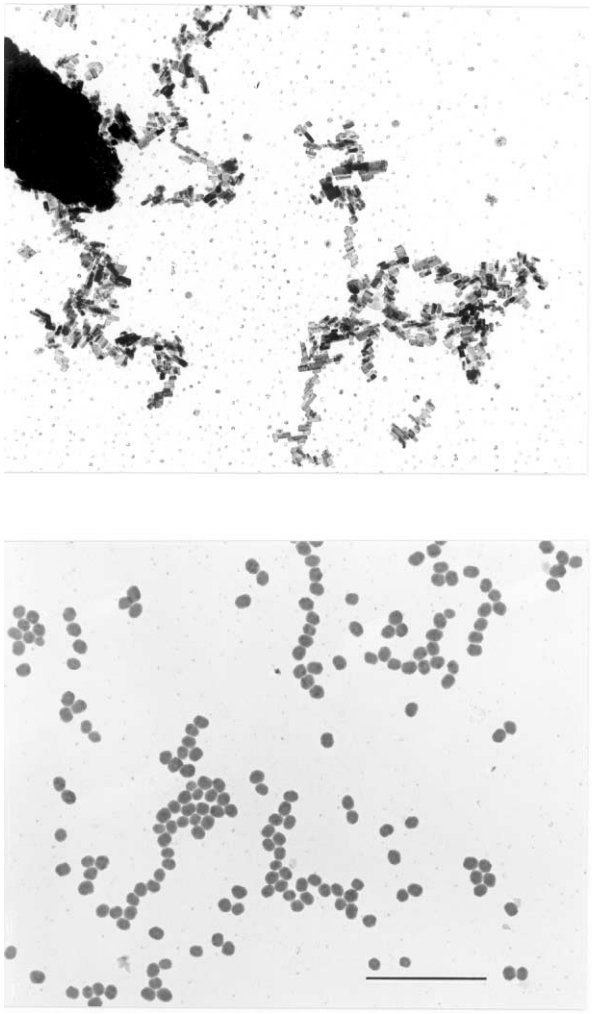

Fig. 8. Morphology of flavanthrone crystals (a) and PTFE particles (b) used in the present investigation. Transmission electron micrographs, scale bar: 2 μm.

regiodefective structures is very small indeed and, in the present case, is only revealed (possibly) by its nucleating ability.

To conclude this section therefore, it appears that the PVDF regioregularity, which was known from previous studies to affect the crystallization behavior (growth rates, crystallization range, melting and self-nucleation, etc.) has also a marked impact on the nucleation behavior upon partial melting, and therefore on the overall morphology. The differences are induced by, or at least associated with, variations in the regioregularity of the chains, and are particularly visible through the memory effect, i.e. for high concentrations of nuclei.

3.4. Enhanced nucleation of PVDF through crystalline additives

High concentrations of nuclei are much searched for in industrial practice, but are not produced by the lengthy partial melting procedures considered so far. Industry makes use of foreign nucleating additives (NA). These are examined in the present section, and their impact shown to be comparable to, if not as good as, self-nucleation.

The efficiency of heterogeneous nucleating additives depends on favorable interactions of the crystalline lattices of substrate and polymer (generally of epitaxial character [18] for non-reactive polymers such as polyolefins or PVDF), and on good dispersion in the polymer: 10^{12} particules/cm^3 are needed to reach final spherulite diameters of ≈1 μm. Such levels of dispersion can be reached by melting and recrystallization of the NA in the polymer. This is the case for the gelifying agent dibenzylidene sorbitol (DBS) [20], in which case good compatibility with the polymer melt is also required. For the insoluble and high melting PTFE [11] and Flavanthrone [10] NAs considered in this paper, only the initial particle or crystal size is a determining criterion, together with means to achieve good dispersion of these particles in the polymer melt (Fig. 8). In this respect, our procedure of blending polymer latexes of PVDF and PTFE appears to be an efficient and industrially viable means to reach high levels of dispersion of the nucleating agents. These two aspects (interactions and dispersion) are now discussed and described in terms of overall nucleation efficiencies, and summarized in Table 3.

3.4.1. Polymer-nucleating agent interactions

Our analysis of NA/polymer interactions was faced with limited success. As indicated in the experimental part, crystals of flavanthrone are too small to perform any meaningful electron diffraction of composite NA/polymer films. Flavanthrone is clearly an efficient NA for PVDF, as judged by the conspicuous development of a transcrystalline layer on its crystal edges, visible in optical microscopy.

Table 3
Impact of PTFE (low molecular weight material) and flavanthrone nucleating additives on the crystallization process of the three grades of Kynar samples. The impact is determined by the increase in T_c relative to a non-nucleated sample (first column); this increase is translated in efficiencies (E) expressed as a percentage of the increase in T_c obtained for a self-nucleated sample

Sample	Kynar 740	+0.1% PTFE	+0.5% PTFE	+1% PTFE	+0.5% Flav	Kynar 1000	+1% PTFE	+5% PTFE	+20% PTFE	+35% PTFE	Kynar 500	+0.5% PTFE
T_c (°C)	132.0	142.7	143.4	143.5	143.5	131.8	144.2	144.7	144.7	144.2	123.9	137.8
E (%)	0	77.5	82.6	83.3	83.3	0	76.1	79.1	79.1	76.1	0	73.2

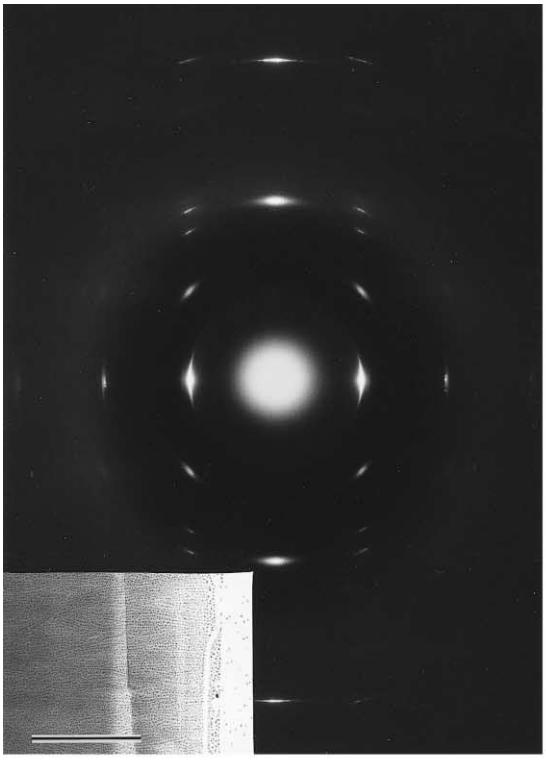

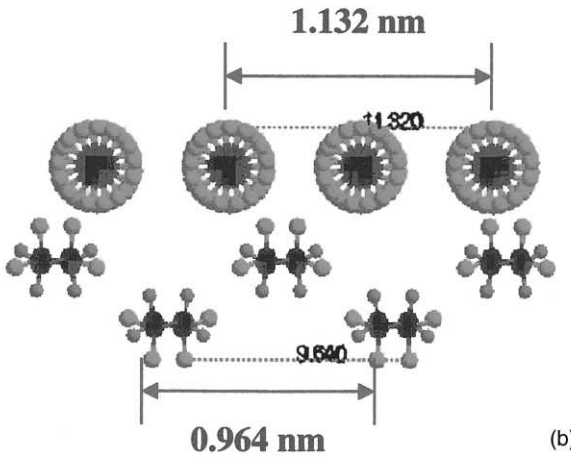

Fig. 9. PVDF/PTFE interactions. (a) Electron diffraction pattern of a bilayer of PVDF deposited, melted and recrystallized on an oriented film of PTFE. PTFE and PVDF chain axes vertical. On the meridian, the outer and inner reflections correspond to 0015_{PTFE} and 002_{PVDF}. Inset: bright field electron micrograph of the edge of a PTFE/PVDF film, in which the top surface of the PVDF has been gold decorated. Scale bar: 0.5 μm. (b) Schematic representation of the PVDF/PTFE interactions at the contact surface, seen along the polymer chain axes. Note the difference in composition of opposite sides of the PVDF layer. Fluorine–fluorine interactions are assumed to be more favorable [13], thus the orientation of the layer displayed here.

Analysis of the PTFE/PVDF double layers (Section 2) yields a composite diffraction pattern of both polymers (Fig. 9). Location of both the 0015_{PTFE} and 002_{PVDF} reflections on the meridian indicates that the PTFE and PVDF chain axes are parallel. Observation of the gold-decorated layers of PVDF epitaxially crystallized on PTFE confirms the above analysis: the PVDF lamellae are oriented at right angle to the PTFE chains. The gold particles, condensed in the interlamellar zones, generate a linear grating, which makes it easy to measure the overall lamellar thickness: ≈160 Å (Fig. 9a, inset). Assuming a (reasonable) 50% overall crystallinity, this figure must be equipartitioned between the crystalline core and amorphous interlayer part.

In a further analysis of the epitaxy, the presence of $0k0$ reflections on the equator indicates that the bc_{PVDF} plane is in contact with PTFE. As this plane does not provide the best possible lattice match with the PTFE substrate we must assume, following the suggestion of Meyer [13], that it is nevertheless selected because it offers — on one of its sides at least — a face highly enriched in fluorine atoms, which are presumably more favorable for interactions with PTFE (Fig. 9b).

3.4.2. Dispersion of the nucleating agents: blending

Dispersion of the NA depends critically on the particle size. Flavanthrone produces 'spontaneously' small crystals (Fig. 8a). For nascent PTFE, this size depends on the polymerization conditions, and more precisely, as established by Seguchi et al. [20], on the concentration of emulsifier used in the polymerization process. Beyond 2%, the polymerization yields fibrils with 200 Å average radius. At or below 1%, rods 300–600 Å in diameter and a few μm long are formed. At even lower concentrations of emulsifier, spherical particles are produced, which are often in the form of folded ribbons with overall 0.1–0.5 μm diameter.

The available, commercial grades of PTFE used in the present study are not the most finely divided ones; however, as shown in Fig. 8b, the average size of the particles (or ribbons) is 0.2–0.3 μm. This size corresponds to 10^{14} particles/cm^3 or, if ideally dispersed in PVDF, 10^{12} for a 1% concentration — somewhat beyond figures obtained by the self-nucleation procedure.

The crystallization behavior of PVDF samples nucleated with these nucleating agents indicates that such a high level of dispersion has not actually been reached. This conclusion is suggested by the location of the peak crystallization temperatures within the crystallization range, i.e. on the efficiency scale established previously. All three Kynar samples have been investigated, and their observed T_c suggest that the efficiency reached with both PTFE and Flavanthrone nucleating agents is always beyond 65% and even beyond 80%. The variation of T_c with concentration of additive yields the expected saturation of the nucleating ability at or around 1% concentration. In a test experiment, a sample of PVDF has been 'saturated' with 35% PTFE, much in the spirit of a similar experiment performed long ago by Beck [21]: the crystallization peak remains nearly unaffected.

To summarize, the above results are very informative about experimental conditions used in this study and

about preferable processing conditions for nucleated samples:

- Both PTFE and Flavanthrone are excellent NA for PVDF. However, flavanthrone has a distinct orange color, which may restrict its use. PTFE is 'neutral' in this respect.
- Although we are dealing with small particle sizes, the dispersion achieved by simple mixing and blending of PTFE and PVDF latexes is 'insufficient' and does not help express the full nucleating potential of the additive. Given the average PTFE latex particle size and concentrations used, about 10^{12} nuclei/cm^3 PVDF would be expected. The actual concentration is smaller, suggesting some form of aggregation of the PTFE particles in the so-called 'powder' sample.
- Very good nucleation efficiencies have been reached in the present study, but even higher efficiencies may be within reach. The use of PTFE particles of much smaller size, such as rods produced (so far only on an experimental basis) by irradiation in the presence of higher concentrations of emulsifier would help achieve even higher degrees of dispersion (probably by a factor of 10). Also, their elongated shape (as opposed to the rounded one in our samples) could be a favorable (although only marginal) geometrical factor.

4. Conclusion

Self-nucleation and heterogeneous nucleation of PVDF samples performed in the present work yield a consistent pattern. It can be summarized as follows:

- Self-nucleation experiments indicate that the Kynar samples investigated (and most probably PVDF in general) have a rather high concentration of foreign (heterogeneous) nuclei, typically in the 10^7/cm^3 range. Conversely, 'ideally' self-nucleated PVDF have 3–4 $\times$ 10^{10} nuclei/cm^3, which corresponds to an average spherulite diameter of 4 μm. This diameter is relatively large (nuclei concentration small), since nuclei concentrations at least 10 times higher should be accessible.
- In one PVDF sample at least (Kynar 500), a permanent memory effect is observed: the nuclei produced during partial melting keep a memory of their orientational relationship within their parent spherulites. Recrystallization restores the overall initial spherulitic pattern, but each spherulite is subdivided in smaller spherulitic entities. A correlation can be established between the permanent memory effect and the existence of a gel fraction in the sample, itself apparently linked to a higher head to head concentration of defects in the chain.
- Flavanthrone and PTFE are very efficient nucleating additives for PVDF. This efficiency is in great part linked with a very small 'grain' size (of crystals for flavanthrone, of latex particles for PTFE). As regards PTFE, the coagulation of blends of PTFE and PVDF latexes procedure used in the present investigation is perfectly adapted to industrial practice. It does not yield the anticipated dispersion of PTFE particles, suggesting that some form of agglomeration takes place: further increase of the nucleating efficiency might be envisaged for better dispersions.
- Alternatively, these efficiencies might be improved by using smaller-sized PTFE particles produced in the presence of higher concentrations of emulsifier. As such, however, the present study shows that it is possible to significantly enhance the crystallization process of plain PVDF. Moreover, as developed in the companion paper [4], these nucleating agents modify significantly both the crystallization kinetics and the physical properties of PVDF blended with amorphous acrylic and methacrylic polymers.

Acknowledgements

The generous financial support of ELF Atochem is gratefully acknowledged. Thanks are also due to Dr Claude Picot, Bernard Meurer and Suzanne Zehnacker for their help in low angle light scattering, NMR and DSC characterizations, respectively.

References

[1] Thierry A, Straupé C, Lotz B, Wittmann JC. Polym Commun 1990;31:299.
[2] Friedrich K. Prog Coll Polym Sci 1978;64:103.
[3] Lovinger A. In: Bassett DC, editor. Developments in crystalline polymers. Applied Science, 1982. Chap. 5.
[4] Schneider S, Drujon X, Wittmann JC, Lotz B. Polymer 2001;42:8799.
[5] Fillon B, Lotz B, Thierry A, Wittmann JC. J Polym Sci B, Polym Phys 1993;31:1395.
[6] Fillon B, Wittmann JC, Lotz B, Thierry A. J Polym Sci B, Polym Phys 1993;31:1383.
[7] Fillon B, Thierry A, Lotz B, Wittmann JC. J Therm Anal 1994;42:721.
[8] Shirai M. Japanese Patent to Kureha Chem Ind Ltd, Shô 48-34 956, 1973.
[9] Segawa M, Iwaki K. US Patent 3 701 749 to Kureha Ltd; 1972.
[10] Lutringer G, Meurer B, Weill G. Polymer 1991;5:885.
[11] Cais RE, Kometani JM. Macromolecules 1985;18:1357.
[12] Wittmann JC, Smith P. Nature 1991;352:414.
[13] Meyer S. Thesis. Strasbourg: University Louis Pasteur; 1995.
[14] Blundel DJ, Keller A, Kovacs AJ. J Polym Sci B, Polym Lett 1966;4:481.
[15] Vidotto G, Levy D, Kovacs AJ. Kolloid ZuZ Polym 1969;230:289.
[16] Fillon B. Thesis. Strasbourg: University Louis Pasteur; 1989.
[17] Loos L. Thesis. Strasbourg: University Louis Pasteur; 1995.
[18] Wittmann JC, Lotz B. Prog Polym Sci 1990;15:909.
[19] Bassett DC. Phil Trans R Soc Lond A 1994;348:29.
[20] Seguchi T, Suwa T, Tamura N, Takeshita M. J Polym Sci, Polym Phys Ed 1974;12:2567.
[21] Beck HN. J Appl Polym Sci 1967;11:673.